#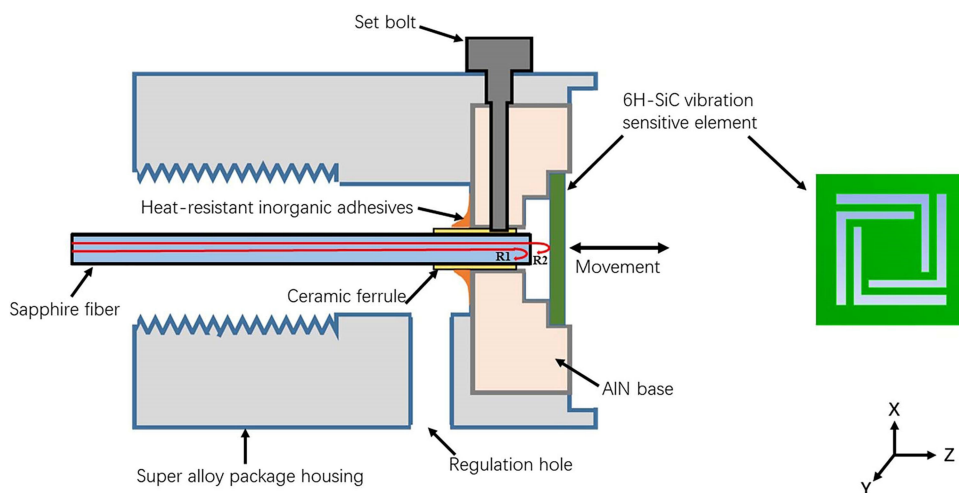 Design, Fabrication, Characterization, and Application of an Ultra-High Temperature 6H-SiC Sapphire Fiber Optic Vibration Sensor

Yigang Huang
Fei Tang
Dawei Ma
Zhenjun Liu
Xiaohao Wang

IEEE

Design, Fabrication, Characterization, and Application of an Ultra-High Temperature 6H-SiC Sapphire Fiber Optic Vibration Sensor

Yigang Huang, Fei Tang [ID], Dawei Ma, Zhenjun Liu, and Xiaohao Wang

State Key Laboratory of Precision Measurement Technology and Instruments, Department of Precision Instrument, Tsinghua University, Beijing 100084, China

Abstract: A 6H-SiC Sapphire fiber optic vibration sensor that can work at 1200 °C was designed, fabricated and tested in this paper. A sapphire fiber and a 6H-SiC vibration-sensitive element constituted the Fabry–Perot resonant cavity. The laser was input via the sapphire fiber, enabling the vibration signal to be converted to an optical signal through the Fabry–Perot cavity, and the vibration parameters were obtained by optical demodulation. The vibration-sensitive element consisted of a cantilever structure, whose structure parameters were determined by the combination of theoretical analysis and simulation. A nanosecond laser was employed to fabricate the 6H-SiC vibration-sensitive element to improve the processing efficiency and simplicity. The sensor was tested from room temperature to 1200 °C. The results showed that its frequency measurement sensitivity remains 0.9997 Hz/Hz from room temperature to 1200 °C, with the full-scale precision being 0.44% F.S. The sensor's output voltage is linearly correlated with the vibration acceleration from ambient temperature to 800 °C, making the acceleration measurement sensitivity 17.86 mV/g at 800 °C. The maximum frequency measurement error was 4.72 Hz when the sensor was at the field application of high temperature casting.

Index Terms: 6H-SiC, ultra-high temperature, sapphire fiber vibration sensor, Fabry-Perot interferometer, laser processing.

1. Introduction

Vibration measurement and analysis is an important topic in numerous fields such as structural engineering, acoustics, biotechnology, entertainment equipment, and security monitoring [1]. To monitor the condition of core components in real time, thus ensuring high performance and reliability, the requirements for vibration measurement under high temperature have become extremely high in fields like aerospace, automobile, and industrial engineering. This requires the sensor to be able to work normally under ultra-high temperature ($>$1,000 °C) for at least 100,000 hours [2]. Conventional vibration sensors based on the piezoelectric principle suffer from limited linear output at high temperature, because most piezoelectric materials (e.g., piezoelectric ceramic) are burdened with phase transition under high temperature (above the Curie point), causing the reduction of the

piezoelectric property or resistivity [3], [4]. In addition, piezoelectric sensors are likely to be disturbed by high temperature bonding failure and electromagnetic interference. Generally, the operating temperature of piezoelectric sensors is around 400 °C [5]. Special high-temperature piezoelectric single-crystal materials have a complex production process and high cost, and their piezoelectric properties and performance against critical shock and vibration are poor [6]–[8], causing them to still be far from high temperature vibration application. Fiber optic sensors based on optical signal transmission are highly sensitive and can effectively solve the high temperature bonding failure of traditional electronic sensors, and meanwhile bring advantages such as corrosion resistance and anti-electromagnetic interference [9]–[11]. Thus they are deemed by many researchers to be the best solution of obtaining measured data in severe environments [12]. Among all the fiber optic sensors, the optical fiber Fabry–Perot interferometer sensor is the most attractive, thanks to its simple principle, structure, small size etc. [13]–[15].

Optical fiber Fabry–Perot interferometer sensors have been widely studied in the field of vibration measurement [16]–[19]. The F–P cavity of common F–P vibration sensors is composed of silica fiber and/or silicon microstructure. Seat *et al.* [20] introduced an extrinsic fiber Fabry–Perot interferometer sensor for measuring vibration speed and displacement, which is relatively insensitive to slight temperature disturbance between 19 °C and 30 °C. Zhang *et al.* [21] proposed an all-fiber vibration sensor based on the Fabry–Perot interferometer structure, by eroding the optical fiber with hydrofluoric acid to fabricate a cantilever-mass block structure, achieving vibration measurement between 20 °C and 120 °C. André *et al.* [22] processed the optical fibers in combination with hydrofluoric acid eroding and a focused ion beam (FIB) to produce a fiber optic vibration sensor, so as to realize measurement between 100 °C and 550 °C. However, F–P fiber optic vibration sensors with a working temperature of above 1,000 °C have not been reported yet. A major reason is that silica has a low melting point and ordinary silica fiber sensors cannot work at temperatures higher than 1,100 °C [23]. Additionally, the mechanical property of silicon begins to deteriorate at 600 °C, becoming liable to plastic deformation [24], thus it is hard for an F–P cavity fabricated with silicon microstructure to work in an environment above 600 °C.

Sapphire fiber boasts advantages such as a high melting point (2,040 °C), small size, high rigidity, anti-corrosion and anti-electromagnetic interference, and is therefore especially suitable for high-temperature sensing under severe environments [25]. A temperature sensor fabricated with sapphire fiber has already realized temperature measurement at 1,880 °C [26]. Silicon carbide (SiC) has excellent thermal, mechanical and optical properties and can be easily combined with optical interferometry [27]. The SiC-based temperature sensor has achieved temperature measurement between ambient temperature and 1,000 °C [28]. Hence, an F–P fiber optic vibration sensor for ultra-high temperature application can be fabricated by combining the high-temperature properties of sapphire fiber and silicon carbide.

In this paper, a 6H-SiC Sapphire Fiber Optic Vibration Sensor (SSFOVS) was proposed, whose F–P cavity is composed of a sapphire fiber and a 6H-SiC vibration-sensitive element to realize the vibration measurement in severe environments such as ultra-high temperature and uncertain electromagnetic interference. A nanosecond laser was employed to fabricate the 6H-SiC cantilever structure. A sapphire fiber was used to receive and transmit the vibration signal. The influence of the nanosecond laser parameters on 6H-SiC processing was investigated. The sensor was tested under ambient temperature (25 °C) and ultra-high temperature (600 °C–1200 °C) respectively, and has been successfully applied in on-site high-temperature casting.

2. Design and Modelling

The SSFOVS is composed of a sapphire fiber, an aluminium nitride (AIN) base, a 6H-SiC vibration-sensitive element, and a super-alloy package housing, as shown in Fig. 1. The Fabry–Perot resonant cavity is constituted by the sapphire fiber and the 6H-SiC vibration-sensitive element. The sapphire fiber's transmission direction is vertical to the internal surface of the vibration-sensitive element under the static condition; during the vibration of the vibration-sensitive element, the length of the F–P cavity changes. The light from the narrow-band laser source shoots into the F–P cavity via the fiber
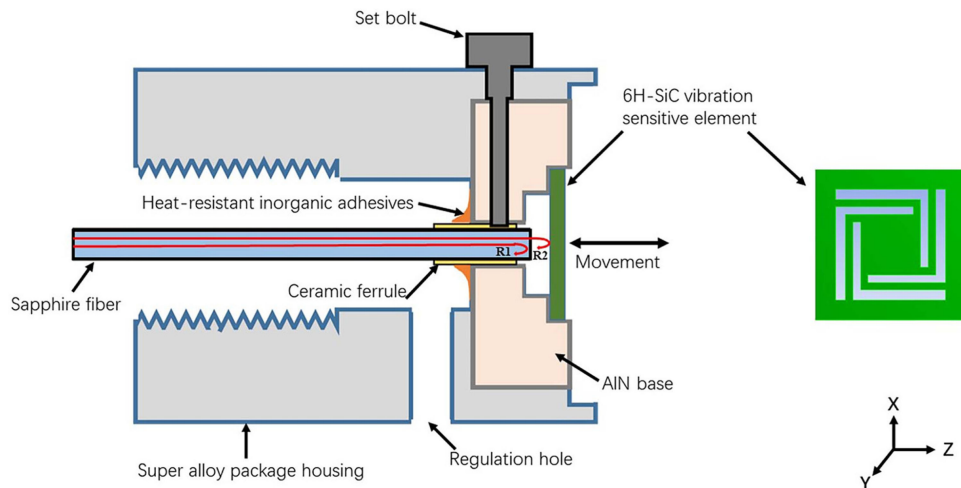
Fig. 1. Structure diagram of 6H-SiC sapphire fiber optic vibration sensor.

and reflects multiple times in the cavity, thus generating resonance and multi-beam interference. The intensity of the interference spectrum varies with the vibration and is obtained by optical demodulation. The vibration parameters were output as voltage after photovoltaic conversion. AlN is adopted as the base of the 6H-SiC vibration-sensitive element, as its thermal expansion coefficient $(4.1 \times 10^{-6}/K)$ is close to that of 6H-SiC $(4.0 \times 10^{-6}/K)$, while it has favourable thermal conductivity, mechanical strength, thermal shock resistance, and thermal stability [29] and can thus effectively reduce the mechanical thermal stress mismatch. The 6H-SiC vibration-sensitive element is embedded in the groove of the step structure in the center of the AlN base, the fiber ceramic ferrule is fixed in the central hole of the AlN base, and the sapphire fiber end face is parallel to the lower surface of the vibration-sensitive element, thus forming the F–P resonant cavity. The location of the ceramic ferrule is adjusted through the regulation hole, to ensure the F–P interference. The bolt passes through the housing and the hole on the side of the AlN base to press against the ceramic ferrule, preventing loosening of the ferrule and the base. The centrosymmetric four-L-shaped cantilever-central mass block structure is adopted for the vibration-sensitive element, with the thickness of the central mass block and the cantilever being the same. This structure ensures that the central mass block has the strongest vibration in the direction vertical to the fiber and reduces the impact of vibration in other directions on the intensity of the reflected interference spectrum, which helps to improve the measurement accuracy. The interference spectrum is transmitted via the sapphire fiber, realizing the measurement from ambient temperature and ultra-high temperature.

The frequency response of the SiC vibration-sensitive element is very important to the dynamic range of the vibration sensor. According to the operating principle of the vibration sensor, the elastic beam of the sensor converts the external acceleration into corresponding mechanical deformation, which is equivalent to a spring-damping system. The calculation formula of the first natural frequency of the spring-damping system is

$$f_0 = \frac{1}{2\pi}\sqrt{\frac{K}{m}} \tag{1}$$

where f_0 is the first natural frequency (Hz) of the cantilever, K is the elastic coefficient (N/m) of the cantilever structure, and m is the mass (kg) of the mass block.

When the four-cantilever folded beam is simplified to a cantilever of rectangular section, its elastic coefficient is

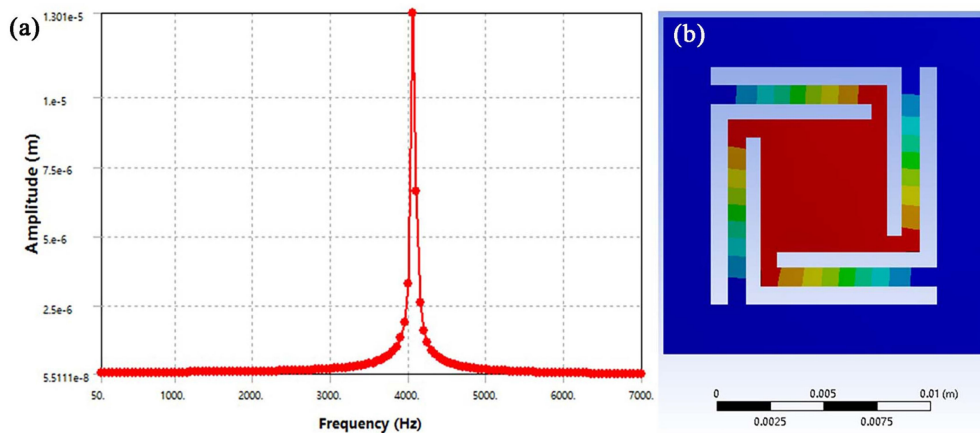$$K = \frac{\lambda E b h^3}{L^3} \tag{2}$$

Fig. 2. The simulation result of the designed SiC vibration sensitive element by ANSYS software: (a) the simulative analysis of the sensitive element's harmonic response; (b) the simulative analysis of the sensitive element's deformation at the first-order modal frequency.

where E is the Young's modulus (Pa) of the material, b is the width (m) of the elastic beam, h is the thickness (m) of the elastic beam, L is the length (m) of the elastic beam, and λ is the calculation constant of the four-cantilever structure.

The mass of the square central mass block is

$$m = a^2 h \tag{3}$$

where a is the side length (m) of the central mass block and ρ the density (kg/m^3) of the material.

The relation between the first natural frequency and structure parameters of the sensitive element structure can be calculated with formulas (1), (2) and (3) as

$$f_0 = \frac{h}{2\pi} \sqrt{\frac{\lambda E b}{a^2 \rho L^3}} \tag{4}$$

Considering the common application requirements for vibration measurement, the operating frequency range of the SSFOVS is designed to be from 100 Hz to 1,000 Hz, so that the resonant frequency of the vibration-sensitive element shall be ensured above 3 kHz. The size of the sensitive element was preliminarily estimated with formula (4); and the ideal first natural frequency of the vibration-sensitive element was later gained through ANSYS finite element simulative analysis, as shown in Fig. 2. The four sides of the sensitive element are set as fixed constraints, while other locations have no constraint; a sine acceleration whose maximum is 20 g was applied to the direction vertical to the central mass block surface. The simulation result shows that when the sensitive element has a thickness of 0.33 mm and a side length of 15 mm, the cantilever has a length of 8.5 mm and a width of 0.75 mm, and the central mass block has a side length of 6 mm, while the resonant frequency is 4,067 Hz, as shown in Fig. 2(a), which satisfies the design requirement for the operating frequency range. Within the operating frequency range of 100–1,000 Hz, the maximum vertical displacement of the central mass block upon the acceleration of 20 g is 87 nm, which meets the optical demodulation requirement that the length of the F–P resonant cavity should be shorter than 100 nm. Fig. 2(b) is the first mode simulation result of the sensitive element, showing the maximum amplitude of the central mass block.

3. Sensor Fabrication

Laser processing, as a highly efficient micromachining method, has high lateral resolution, low thermal effect, high flexibility and can be used for micro-nano machining of fiber optic sensors [30]–[33]. We fabricated the vibration-sensitive element of SSFOVS by processing a 2-inch 6H-SiC
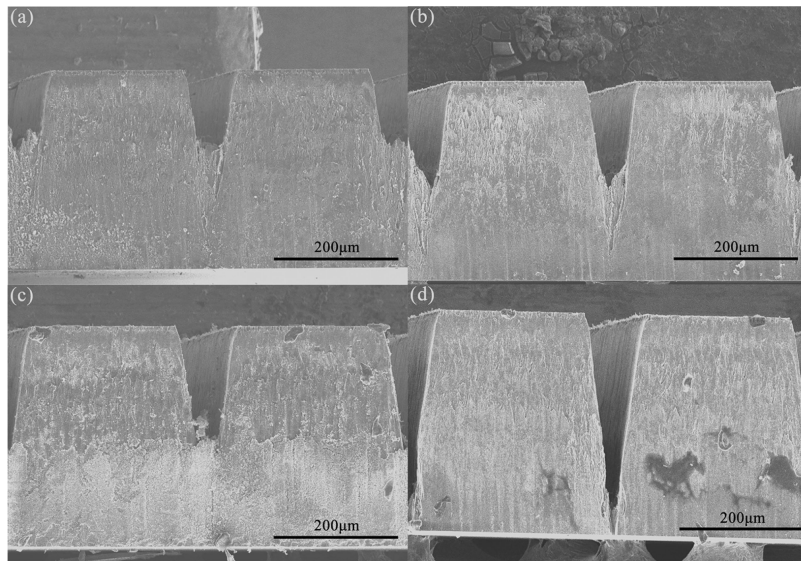
Fig. 3. SEM Image of Laser Processing of 6H-SiC. (a–d) Times of laser scanning: (a) 3 times, (b) 4 times, (c) 5 times, (d) 6 times.
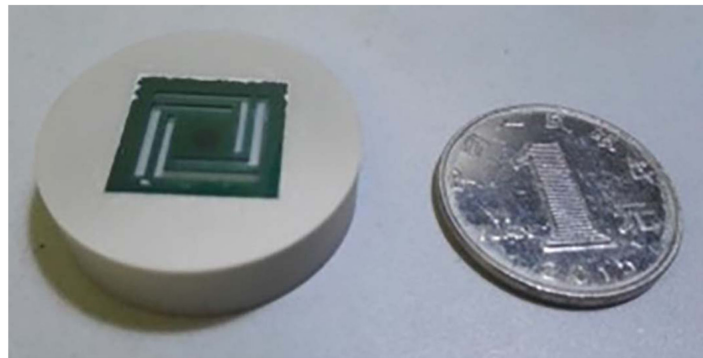

Fig. 4. The 6H-SiC Vibration-sensitive Element Fixed in the AIN Base.

wafer (Tankeblue, China) with an ultraviolet nanosecond laser (Chutian laser, China). With the laser wavelength of 355 nm and constant 5W laser power, scanning at the fixed speed of 1,000 mm/s was conducted on the surface of the 6H-SiC wafer. Each scan left a wedge groove on the surface of the wafer. Under the constant laser power and scanning speed, each scan increased the groove depth by about 40 um, as shown in Fig. 3. After 9 times scanning, the 6H-SiC vibration-sensitive element of four-cantilever-central mass block structure was obtained. The average processing time of a single 6H-SiC vibration-sensitive element is about 4min. Ultrasonic-assisted processing was adopted for the AIN base to obtain the step-type square groove and the central hole. Fig. 4 shows the processed 6H-SiC vibration-sensitive element stuck to the square groove of the AIN base by the heat-resistant inorganic adhesive aluminosilicate.

The structure of SSFOVS after packaging is shown in Fig. 5. Nickel-base super alloy, which has high plasticity, high durable creep strength, and favorable resistance to oxidation [34], was chosen as the housing material. The AIN base with the vibration-sensitive element was placed in the housing, through the lower part of which the fiber ceramic ferrule was inserted into the central hole of the AIN base. When the interference was favorable by adjusting the location of the fiber ceramic ferrule, the bolt was inserted through the housing and the side hole of the AIN base to

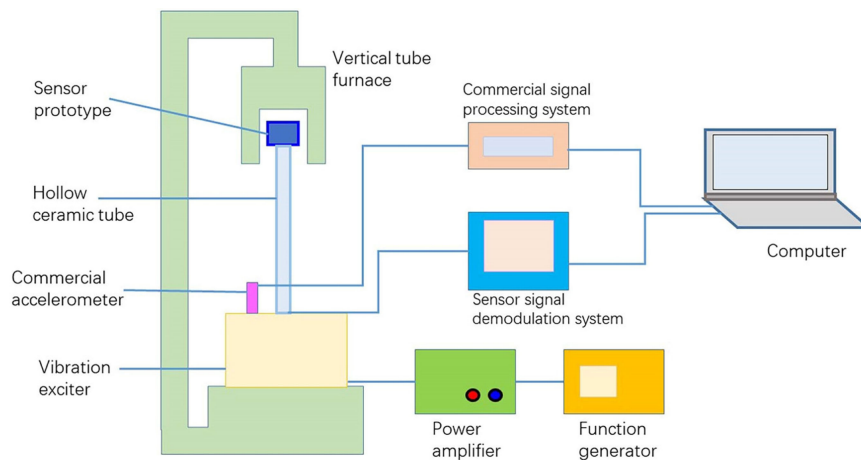Fig. 5. Sample of 6H-SiC sapphire fiber optic vibration sensor connected with the hollow ceramic tube.

Fig. 6. Schematic diagram of the experimental facility of high-temperature vibration test.

fix the ceramic ferrule. Aluminosilicate inorganic adhesive was then used to double fix the ceramic ferrule to the AIN base at the bottom.

4. Characterization and Discussion

Fig. 6 shows the experimental facility of the high-temperature vibration test, mainly including a signal generator, a vertical tube furnace, a signal demodulator, a vibration exciter, and a power amplifier. The sensor is connected with a vibration exciter (Sinocera Piezotronics, China) via a zirconia ceramic tube, and is completely inside the customized vertical tube furnace (Shanghai Institute of Optics and Fine Mechanics, China), whose maximum internal temperature is up to 1,400 °C, with a regulation precision of 1 °C. The fiber is drawn out of the zirconia hollow ceramic tube and connected to the demodulation system, which can collect the full waveform of interference spectrum output from the sensor and display it on the computer. The sine signal is generated by the function generator (Tektronix, US), amplified by the power amplifier (Sinocera Piezotronics, China), and then applied to the vibration exciter to produce the required vibration. The output acceleration of the exciter is measured by a commercial accelerometer (PCB Piezotronics, US)
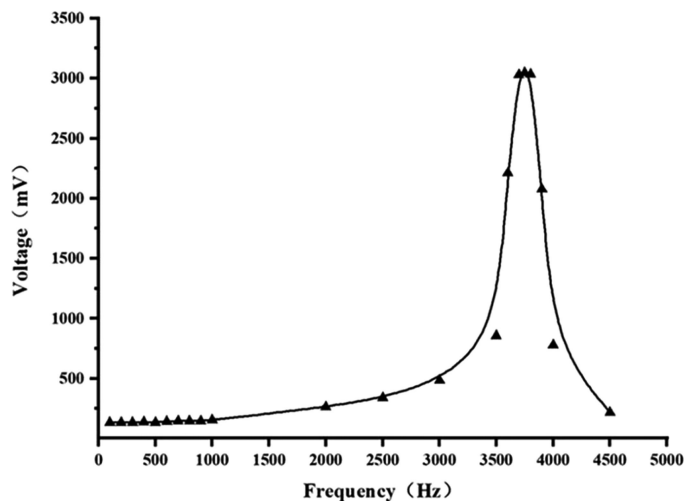
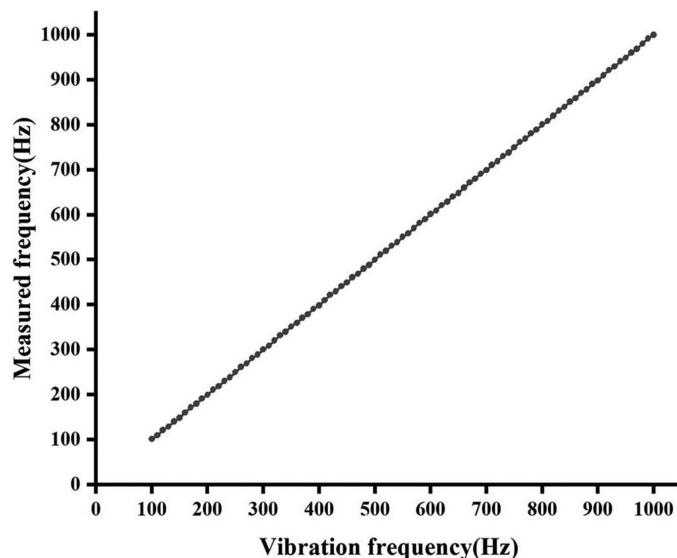Fig. 7. Frequency response of 6H-SiC sapphire fiber optic vibration sensor.

Fig. 8. Frequency measurement of 6H-SiC sapphire fiber optic vibration sensor at 1,200 °C.

fixed on the vibration surface of the exciter, and a vibration signal testing and analyzing system (Müller-BBM VibroAkustik Systeme, Germany) records and displays the real-time measurement of the acceleration on the computer. The sensor is tested between ambient temperature and 1,200 °C, and its output is recorded.

Fig. 7 shows the frequency response of the SSFOVS between 100 Hz and 4,500 Hz at room temperature. It is observed that the resonant frequency is around 3,750 Hz, quite close to the first natural frequency (4,067 Hz) of the vibration-sensitive element obtained in the ANSYS simulation. The operating frequency range is 100 Hz–1 kHz, which satisfies the design requirement. The frequency measurement experiment was carried out within the frequency range of 100 Hz–1 kHz, with a step length of 10 Hz, at ambient temperature, 600 °C, 800 °C, 1,000 °C, and 1,200 °C, respectively. The frequency measurement result for the SSFOVS at 1,200 °C is illustrated in Fig. 8. It indicates that the measured frequency of the SSFOVS is of extremely high linearity with the vibration frequency, with the frequency measuring sensitivity of 0.9997 Hz/Hz, the maximum error
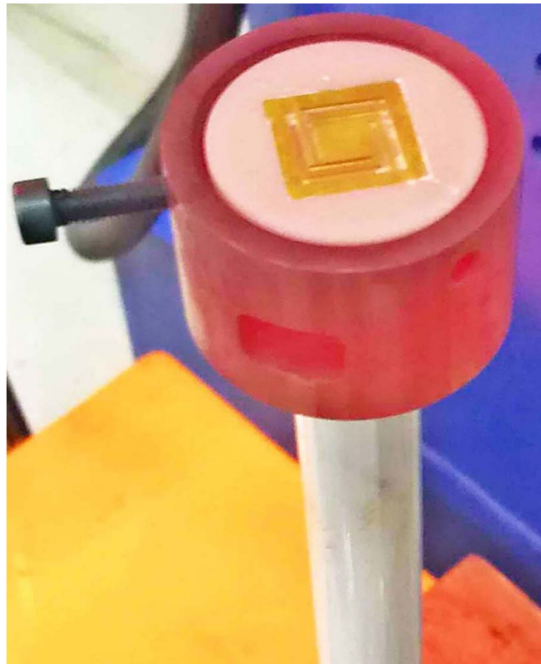
Fig. 9. The sensor taken out of the furnace right after the 1,200 °C vibration test.

of 4 Hz, and the full scale precision of $4/(1,000–100)*100\% = 0.44\%$ F.S. The results at ambient temperature, 600 °C, 800 °C, and 1,000 °C remain the same, indicating that the frequency measuring function of the SSFOVS is not affected by temperature. The frequency measuring sensitivity and full-scale precision of the SSFOVS still remain the same when the input vibration acceleration changes from 1 g to 5 g. The sensor taken out of the furnace right after the 1,200 °C high-temperature test is still in good shape, and the silicon carbide vibration-sensitive element is intact, as shown in Fig. 9.

Fig. 10 shows the relation between the acceleration and the SSFOVS' output voltage at 800 °C within the vibration frequency of 100–1,000 Hz, with the acceleration ranging from 1 g to 5 g. It shows that the output voltage increases linearly with the applied acceleration, with the nonlinearity of 1.22%, 3.36%, −11.16%, −5.87%, 4.96% and 7.97% for frequency of 100 Hz, 200 Hz, 400 Hz, 600 Hz, 800 Hz, and 1,000 Hz respectively. The inset of Fig. 10 displays the sensor's acceleration measurement sensitivity (the slope of the curves in Fig.10) under various frequencies, namely 18.91 mV/g, 18.33 mV/g, 15.14 mV/g, 11.99 mV/g, 17.86 mV/g, and 16.44 mV/g at 100 Hz, 200 Hz, 400 Hz, 600 Hz, 800 Hz, and 1,000 Hz respectively. It can be seen that the sensor's acceleration measurement sensitivity maintains relatively stable except at 400 Hz and 600 Hz. The reason may be that the natural frequency of the fixed device (e.g., the hollow ceramic tube) is between 400 and 600 Hz, which affects the sensitivity of the sensor.

At ambient temperature, 600 °C and 800 °C, at the vibration frequency of 800 Hz, the output voltage of the SSFOVS and the acceleration maintain an excellent linear relation, with the nonlinearity of −3.91%, −3.60% and 4.96% respectively, as shown in Fig. 11. This shows that as the temperature increases, the acceleration measurement sensitivity decreases, which is 44.64 mV/g, 31.75 mV/g, and 17.86 mV/g respectively. That is probably because the background light noise under high temperature is relatively strong, leading to the reduced detected intensity of the interference spectrum, and thus the output voltage after photovoltaic conversion decreases accordingly. The linear relation between the output voltage and the acceleration deteriorates when the temperature reaches 1,000 °C or above.
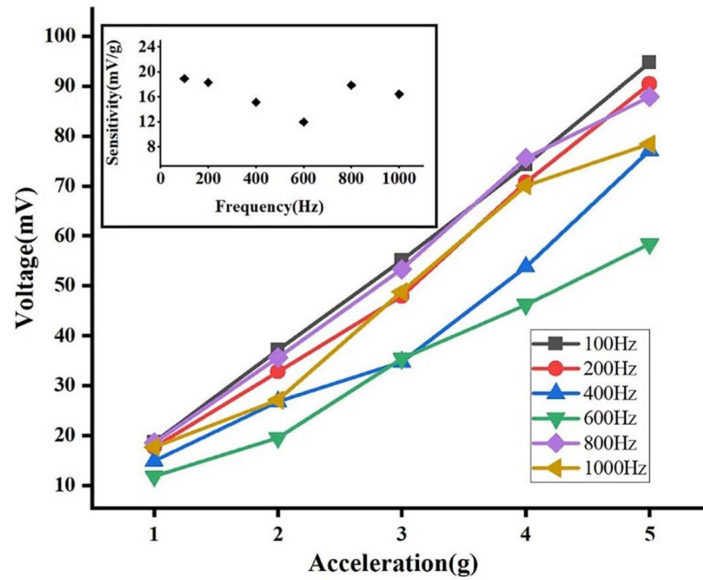
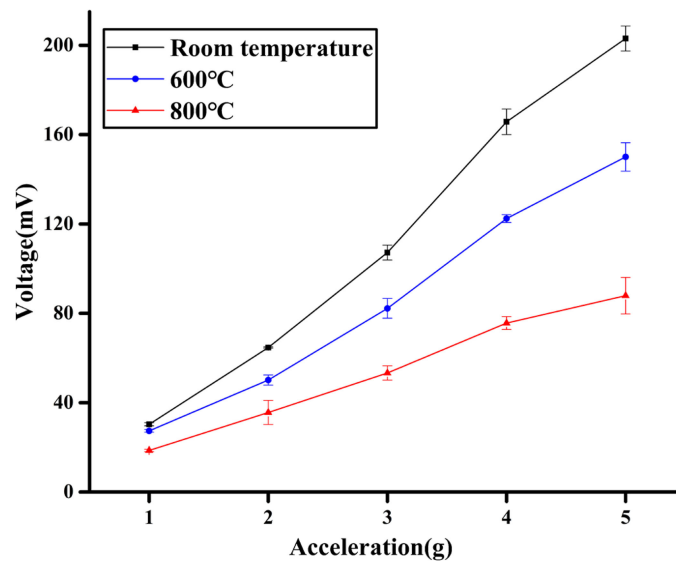Fig. 10. The acceleration measurement within 100–1,000 Hz at 800 °C.

Fig. 11. The acceleration measurement at 800 Hz under ambient temperature, 600 °C and 800 °C. The error bars represent the standard deviation (n = 3).

5. Field Application

Field application of the SSFOVS was carried out in the high-temperature casting workshop of Wuhan Heavy Duty Machine Tool Group Corporation, to verify the high-temperature stability of the sensor in severe environments such as high temperature, dustiness and uncertain electromagnetic interference (there were four large electromagnetic induction furnaces used to melt molten iron in the casting workshop), as shown in Fig. 12. The SSFOVS was installed in a flask. A 10 mm thick steel plate was partly inserted into the mold cavity through a man-made hole, with its left part being able to direct contact the molten iron. The SSFOVS was fitted upside down on the upper surface of the outside part of the steel plate. The pouring of the molten iron in the ladle was not carried out
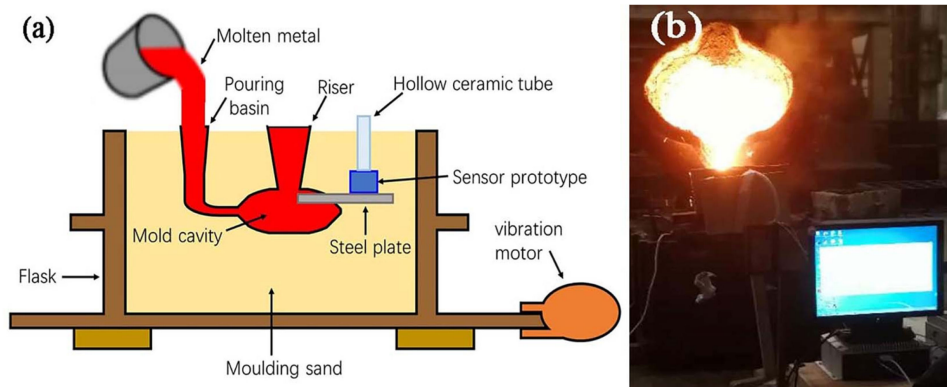
Fig. 12. High-temperature casting field application of the sensor: (a) the location of the sensor in the flask; (b) the experiment site.

TABLE 1
Frequency Measurement Data of Application of the Sensor

Motor rotation speed (rpm)	Motor vibration frequency (Hz)	Sensor measured frequency (Hz)	Frequency measurement error (Hz)
6000	100	102.58	2.58
6300	105	102.06	-2.94
6600	110	109.45	-0.55
7200	120	116.89	-3.11
7500	125	126.37	1.37
7800	130	134.72	4.72

until its temperature was measured to be 1,300 °C. At the same time of the pouring, the vibration motor (Jinan Sigmar, China) clamped at the flask's flange was started, enabling the molten iron to enter the mold cavity under the mold vibration. The vibration continued for another half an hour after pouring. During vibration, the vibration motor speed changes and the vibration frequency was monitored in real time by the SSFOVS.

The motor speed frequency formula is

$$f = \frac{PNs}{120} \tag{5}$$

where f is the vibration frequency in Hz of the motor, P is the number of pole pairs of the motor, and Ns is the shaft rotation speed in rpm of the motor.

Accordingly, the generated vibration frequency of the motor we used (with 2 pole pairs) is theoretically its rotation speed divided by 60. Table 1 shows the field experiment data of the SSFOVS. It can be calculated that the absolute value of the maximum measuring error is 4.72 Hz, which is very close to the laboratory measurement.

6. Conclusion

In this paper, a 6H-SiC Sapphire Fiber Optic Vibration Sensor (SSFOVS) of Fabry–Perot interferometer structure was designed and fabricated, effectively realizing the vibration frequency and

acceleration measurement in an ultra-high temperature environment. Heat-resistant 6H-SiC and sapphire fiber were adopted as the materials for the critical components. The sapphire fiber and the 6H-SiC vibration element constituted the F–P resonant cavity. It was proposed for the first time that the laser process be adopted for SiC to fabricate the vibration-sensitive element, which reduced the process difficulty and increased the efficiency. The sensor has a maximum operating temperature of 1,200 °C; from ambient temperature to 1,200 °C, the frequency measuring sensitivity remains 0.9997 Hz/Hz, with the full-scale precision of 0.44% F.S. The sensor's output voltage and vibration acceleration are linearly correlated between ambient temperature and 800 °C, with the acceleration measuring sensitivity of the sensor at 800 Hz under 800 °C being 17.86 mV/g. The field high-temperature casting test shows that the sensor exhibits a good working performance, with the maximum frequency test error of 4.72 Hz. Compared with traditional vibration sensors, the SSFOVS boasts small size, high sensitivity, and a rapid response, and can work in severe environments such as high temperatures and uncertain electromagnetic interference. It has filled the gap in high-temperature vibration sensors and has a wide prospect of application.

References

[1] B. Ferrer, J. Espinosa, A. B. Roig, J. Perez, and D. Mas, "Vibration frequency measurement using a local multithreshold technique," *Opt. Exp.*, vol. 21, no. 22, pp. 26198–26208, 2013.

[2] K. Kim, S. Zhang, W. Huang, F. Yu, and X. Jiang, "YCa4O (BO3) 3 (YCOB) high temperature vibration sensor," *J. Appl. Phys.*, vol. 109, 2011, Art. no. 126103.

[3] T. Stevenson *et al.*, "Piezoelectric materials for high temperature transducers and actuators," *J. Mater. Sci., Mater. Electron.*, vol. 26, no. 12, pp. 9256–9267, 2015.

[4] S. Zhang and F. Yu, "Piezoelectric materials for high temperature sensors," *J. Amer. Ceram. Soc.*, vol. 94, no. 10, pp. 3153–3170, 2011.

[5] V. Giurgiutiu, B. Xu, and W. Liu, "Development and testing of high-temperature piezoelectric wafer active sensors for extreme environments," *Struct. Health Monit.*, vol. 9, no. 6, pp. 513–525, 2010.

[6] F.-P. Yu *et al.*, "High temperature piezoelectric single crystals: Recent developments," in *Proc. Piezoelectricity, Acoust. Waves, Device Appl. Symp.*, 2016, pp. 1–7.

[7] A. Sehirlioglu, A. Sayir, and C. Klemenz, "High-temperature properties of piezoelectric langatate single crystals," 2007.

[8] S. Zhang *et al.*, "Characterization of piezoelectric single crystal Y Ca 4 O (BO 3) 3 for high temperature applications," *Appl. Phys. Lett.*, vol. 92, no. 20, 2008, Art. no. 202905.

[9] B. H. Lee *et al.*, "Interferometric fiber optic sensors," *Sensors*, vol. 12, no. 3, pp. 2467–2486, 2012.

[10] K. Kesavan, K. Ravisankar, S. Parivallal, P. Sreeshylam, and S. Sridhar, "Experimental studies on fiber optic sensors embedded in concrete," *Measurement*, vol. 43, no. 2, pp. 157–163, 2010.

[11] S. J. Mihailov, "Fiber bragg grating sensors for harsh environments," *Sensors*, vol. 12, no. 2, pp. 1898–1918, 2012.

[12] W. J. Pulliam, P. M. Russler, and R. S. Fielder, "High-temperature high-bandwidth fiber optic MEMS pressure-sensor technology for turbine engine component testing," in *Fiber Optic Sensor Technology and Applications 2001*, Bellingham, WA, USA: SPIE, 2002, vol. 4578, pp. 229—239.

[13] M. Islam, M. Ali, M.-H. Lai, K.-S. Lim, and H. Ahmad, "Chronology of fabry-perot interferometer fiber-optic sensors and their applications: A review," *Sensors*, vol. 14, no. 4, pp. 7451–7488, 2014.

[14] H. Y. Choi, K. S. Park, S. J. Park, U.-C. Paek, B. H. Lee, and E. S. Choi, "Miniature fiber-optic high temperature sensor based on a hybrid structured Fabry–Perot interferometer," *Opt. Lett.*, vol. 33, no. 21, pp. 2455–2457, 2008.

[15] C. Wu, H. Fu, K. K. Qureshi, B.-O. Guan, and H.-Y. Tam, "High-pressure and high-temperature characteristics of a Fabry–Perot interferometer based on photonic crystal fiber," *Opt. Lett.*, vol. 36, no. 3, pp. 412–414, 2011.

[16] T. Yoshino, K. Kurosawa, K. Itoh, and T. Ose, "Fiber-optic Fabry-Perot interferometer and its sensor applications," *IEEE J. Quantum Electron.*, vol. 18, no. 10, pp. 1624–1633, Oct. 1982.

[17] A. Kersey, D. Jackson, and M. Corke, "A simple fibre Fabry-Perot sensor," *Opt. Commun.*, vol. 45, no. 2, pp. 71–74, 1983.

[18] A. Ezbiri and R. Tatam, "Interrogation of low finesse optical fibre Fabry-Pérot interferometers using a four wavelength technique," *Meas. Sci. Technol.*, vol. 7, no. 2, 1996.

[19] A. Gerges, T. Newson, J. D. Jones, and D. A. Jackson, "High-sensitivity fiber-optic accelerometer," *Opt. Lett.*, vol. 14, no. 4, pp. 251–253, 1989.

[20] H. Seat, E. Ouisse, E. Morteau, and V. Metivier, "Vibration–displacement measurements based on a polarimetric extrinsic fibre Fabry–Perot interferometer," *Meas. Sci. Technol.*, vol. 14, no. 6, p. 710, 2003.

[21] Q. Zhang, T. Zhu, Y. Hou, and K. S. Chiang, "All-fiber vibration sensor based on a Fabry–Perot interferometer and a microstructure beam," *J. Opt. Soc. Amer. B*, vol. 30, no. 5, pp. 1211–1215, 2013.

[22] R. M. André *et al.*, "Focused ion beam post-processing of optical fiber Fabry-Perot cavities for sensing applications," *Opt. Exp.*, vol. 22, no. 11, pp. 13102–13108, 2014.

[23] A. H. Choi, *Handbook of Optical Microcavities*. Singapore: Pan Stanford, 2014.

[24] Y. Jiang, J. Li, Z. Zhou, X. Jiang, and D. Zhang, "Fabrication of all-SiC fiber-optic pressure sensors for high-temperature applications," *Sensors*, vol. 16, no. 10, p. 1660, 2016.

[25] G. N. Merberg and J. A. Harrington, "Optical and mechanical properties of single-crystal sapphire optical fibers," *Appl. Opt.*, vol. 32, no. 18, pp. 3201–3209, 1993.

[26] Y. Guo, W. Xia, Z. Hu, and M. Wang, "High-temperature sensor instrumentation with a thin-film-based sapphire fiber," *Appl. Opt.*, vol. 56, no. 8, pp. 2068–2073, 2017.

[27] W. J. Pulliam, P. M. Russler, R. Mlcak, K. A. Murphy, and C. L. Kozikowski, "Micromachined SiC fiber optic pressure sensors for high-temperature aerospace applications," in *Industrial Sensing Systems*, Bellingham, WA, USA: SPIE, 2000, vol. 4202, pp. 21–31.

[28] N. A. Riza and M. Sheikh, "Silicon-carbide-based extreme environment temperature sensor using wavelength-tuned signal processing," *Opt. Lett.*, vol. 33, no. 10, pp. 1129–1131, 2008.

[29] C. Yun, Y. Feng, T. Qiu, J. Yang, X. Li, and L. Yu, "Mechanical, electrical, and thermal properties of graphene nanosheet/aluminum nitride composites," *Ceram. Int.*, vol. 41, no. 7, pp. 8643–8649, 2015.

[30] Y. Zhang, L. Yuan, X. Lan, A. Kaur, J. Huang, and H. Xiao, "High-temperature fiber-optic Fabry–Perot interferometric pressure sensor fabricated by femtosecond laser," *Opt. Lett.*, vol. 38, no. 22, pp. 4609–4612, 2013.

[31] Z. L. Ran, Y. J. Rao, W. J. Liu, X. Liao, and K. S. Chiang, "Laser-micromachined Fabry-Perot optical fiber tip sensor for high-resolution temperature-independent measurement of refractive index," *Opt. Exp.*, vol. 16, no. 3, pp. 2252–2263, 2008.

[32] Y. Zhang, B.-O. Guan, and H.-Y. Tam, "Characteristics of the distributed Bragg reflector fiber laser sensor for lateral force measurement," *Opt. Commun.*, vol. 281, no. 18, pp. 4619–4622, 2008.

[33] Y. Dai, M. Yang, G. Xu, and Y. Yuan, "Magnetic field sensor based on fiber Bragg grating with a spiral microgroove ablated by femtosecond laser," *Opt. Exp.*, vol. 21, no. 14, pp. 17386–17391, 2013.

[34] A. Heckl, S. Neumeier, M. Göken, and R. Singer, "The effect of Re and Ru on γ/γ' microstructure, γ-solid solution strengthening and creep strength in nickel-base superalloys," *Mater. Sci. Eng., A*, vol. 528, no. 9, pp. 3435–3444, 2011.